Environ Earth Sci (2015) 73:2473–2482
DOI 10.1007/s12665-014-3596-8

ORIGINAL ARTICLE

Dynamic response of a thawing soil around the tunnel under the vibration load of subway

Peng-Peng He · Zhen-Dong Cui

Received: 31 December 2013 / Accepted: 8 August 2014 / Published online: 17 August 2014

Abstract A certain thickness of thawing soil remains after the construction of subway tunnel by the artificial freezing method in soft soil area. The physical and mechanical properties of soil change a lot after freezing and thawing; therefore, the dynamic response of thawing soil is different from that of undisturbed soil under the same vibration loads of subway. The numerical simulations of thawing soil and undisturbed soil were conducted in this paper. The variations of the acceleration and the displacement of the surface and some special points were analyzed. The propagation characteristics of wave in the soil and the differences between thawing soil and undisturbed soil were obtained.

Keywords Dynamic response · Thawing soil · Subway vibration · Numerical simulation

Introduction

In recent years, with the rapid increase of population and traffic jams, subway construction has already become an important way to develop underground space and ease traffic jams. In the process of subway construction, especially in some soft soil areas, artificial freezing method has become a common temporary reinforcement method of the foundation. For example, 95 % of the connecting passages in Shanghai were constructed by artificial freezing method. Moreover, artificial freezing method is frequently used in the repair for water inflow and collapse in a shield tunnel. While after the construction of a subway tunnel by artificial freezing method, there is a certain amount of residues of frozen soil, e.g., the remnant frozen soil is about 3–4 m in thickness around the crossing-river tunnel of East Fuxing Road in Shanghai.

The dynamic response of ordinary soil around the tunnel under vibration load has been studied by many researchers by means of various methods, for example, microscopic approach (Tang et al. 2014; Yan et al. 2013). However in general, current researches are mainly concentrated on theoretical analysis and numerical simulation. For relatively simple analytical methods, the whole system is mainly simplified in that different kinds of loads move on the Winkler or the half-space foundation (Dieterman and Metrikine 1997; Kaynia et al. 2000). A more complicated and accurate analytical methodology (PiP model) that considers the major dynamic characteristics of a 3D system for calculating subway vibration was developed by Forrest and Hunt (2006). Moreover, the PiP model was coupled to the track via different supports (Hussein and Hunt 2007). Sheng et al. (2002) presented a method that depends on the boundary integral equations of only the displacement Green's function based on the discrete wavenumber fictitious force method. Lu et al. (2007) presented another model for calculating seismic dynamic response. The model accounted for the problem with piecewise liners embedded in a porous medium. The soil surrounding the tunnel was supposed to be saturated porous medium and was described by Biot's poroelastic theory, and the tunnel was supposed to be the combination of liner pieces and connecting joints which were treated as curved beams and characterized by curved beam theories. Guan and Moore (1994) solved the 3D wave equations for two cylindrical

P.-P. He · Z.-D. Cui (✉)
State Key Laboratory for Geomechanics and Deep Underground Engineering, School of Mechanics and Civil Engineering, China University of Mining and Technology, Xuzhou, Jiangsu 221116, People's Republic of China
e-mail: czdjiaozuo@163.com

cavities in an unbounded medium to account for the interaction between two deep side-by-side circular tunnels.

For numerical simulation, Israil and Ahmad (1989),

Ewing et al. (1958) and Wolf (1985, 1988) concentrated on the dynamic response of soil under the point or line loads. Many researchers also studied the influences of various factors. Lieb and Sudret (1998), Alabi (1992), Yang et al. (2003) and Eason (1965) studied the effect of train speed and depth of soil layer. Rieckh et al. (2012) discussed the dynamic characteristics of layered anisotropic soil under vibration loads. Nejati et al. (2012) studied the influence of subway vibration on the surface through numerical methods and theoretical analysis. Vinson et al. (1978), Vinson and Li (1980) considered the dynamic performance of thawing clay and thawing sandy soil. Ting et al. (1983) researched the dynamic strength of frozen sandy soil based on a large number of statistical data. Vibration from underground railways is frequently modeled by the coupled Finite Element–Boundary Element (FE–BE) technique. Sheng et al. (2006) incorporated the discrete wavenumber method to improve the computational efficiency. Clouteau et al. (2005) developed a numerical model based on FE-BE model for calculating vibration response of subway.

After the construction of artificial freezing, the thawing soil was formed after the melting of the frozen soil and the physical and mechanical properties of soil changed a lot during freezing and thawing. The freezing and thawing weakens the connecting forces between soil particles (Konrad 1989) and increases the permeability of soil (Viklander and Eigenbrod 2000). It also affects the strength and the compressibility of soil (Brams and Yao 1964; Graham and Au 1985). After the freezing and thawing, the permeability of clay (Yang and Zhang 2002) is approximately 3–10 times than that of the undisturbed soil, while the unconfined compressive strength is just about 33–55 % of that of undisturbed soil. The deterioration of soil characteristics will lead to the differences between the dynamic response of thawing soil and undisturbed soil. The thawing soil may be more susceptible to be damaged under the same vibration load; therefore, the kinetic properties and deformation of thawing soil around the subway tunnel are of vital significance for the local stability of the tunnel. However, the researches on the dynamic characteristics of thawing soil are little; only a small amount focuses on the dynamic response under seismic load (Singh and Donovan 1977; Finn and Yong 1978).

In this paper, the 3D governing equations were derived and the solving method was given. The material parameters of the thawing soil and the undisturbed soil used in the numerical simulations were obtained by dynamic triaxial tests. The dynamic response of thawing soil and undisturbed soil in the same environmental conditions were compared and analyzed.

Governing equations

Formulations of the model

In order to simplify the establishment of model equations, the model in this paper is based on the following hypotheses: (1) the strain of the soil and tunnel is small enough so that elastic relation can be applied; (2) the properties of the model remain unchanged in the longitudinal direction, that is the model can be treated as a plane strain problem; (3) the interface of the tunnel and the soil satisfies the deformation compatibility.

The governing equations of the whole model consist of three parts: the tunnel, the soil and their interface. It is assumed that the long-term displacement fields of the model are known. The dynamic perturbation displacements $\mathbf{u}$ due to dynamic loads will emerge, which are sufficiently small so that linear equations can be allowed.

The dynamic strain ε can be expressed by the perturbation displacements $\mathbf{u}$ as follows:

$$\boldsymbol{\varepsilon} = \frac{1}{2}\left[\nabla\mathbf{u} + (\nabla\mathbf{u})^{\mathrm{T}}\right] \tag{1}$$

According to Hooke's law, the dynamic stress $\boldsymbol{\sigma}$ can be calculated by

$$\boldsymbol{\sigma} = \lambda(\nabla \cdot \mathbf{u})E_3 + 2\mu\boldsymbol{\varepsilon} \tag{2}$$

where λ and μ are the Lame constants and they are expressed as $\lambda = \frac{\upsilon E}{(1+\upsilon)(1-2\upsilon)}$ and $\mu = \frac{E}{2(1+\upsilon)}$, in which υ and μ are Poisson's ratio and shear modulus, respectively. E_3 is the 3×3 unit matrix.

The governing equations and boundary conditions of the system in time–space domain can be written as follows.

For the soil:

$$\rho_s \frac{\partial^2 \mathbf{u_s}}{\partial t^2} = (\lambda + \mu)\nabla(\nabla \cdot \mathbf{u_s}) + \mu\nabla^2\mathbf{u_s} + \mathbf{f_s} \tag{3}$$

For the tunnel:

$$\rho_t \frac{\partial^2 \mathbf{u_t}}{\partial t^2} = (\lambda + \mu)\nabla(\nabla \cdot \mathbf{u_t}) + \mu\nabla^2\mathbf{u_t} + \mathbf{f_t} \tag{4}$$

For their interface:

$$\mathbf{u_s} = \mathbf{u_t} \tag{5}$$

$$\boldsymbol{\sigma_s} = \sigma_t \tag{6}$$

Equation solution

As the forms of Eqs. (3) and (4) are the same, only Eq. (3) is solved following. The component forms of Eq. (3) in x, y and z direction can be written as:

$$\rho_s\frac{\partial^2 u_{sx}}{\partial t^2}=(\lambda+\mu)\left(\frac{\partial^2 u_{sx}}{\partial x^2}+\frac{\partial^2 u_{sy}}{\partial x\partial y}+\frac{\partial^2 u_{sz}}{\partial x\partial z}\right)+\mu\left(\frac{\partial^2 u_{sx}}{\partial x^2}+\frac{\partial^2 u_{sx}}{\partial y^2}+\frac{\partial^2 u_{sx}}{\partial z^2}\right)+f_{sx}$$
$$\rho_s\frac{\partial^2 u_{sy}}{\partial t^2}=(\lambda+\mu)\left(\frac{\partial^2 u_{sx}}{\partial x\partial y}+\frac{\partial^2 u_{sy}}{\partial y^2}+\frac{\partial^2 u_{sz}}{\partial y\partial z}\right)+\mu\left(\frac{\partial^2 u_{sy}}{\partial x^2}+\frac{\partial^2 u_{sy}}{\partial y^2}+\frac{\partial^2 u_{sy}}{\partial z^2}\right)+f_{sy}$$
$$\rho_s\frac{\partial^2 u_{sz}}{\partial t^2}=(\lambda+\mu)\left(\frac{\partial^2 u_{sx}}{\partial x\partial z}+\frac{\partial^2 u_{sy}}{\partial y\partial z}+\frac{\partial^2 u_{sz}}{\partial z^2}\right)+\mu\left(\frac{\partial^2 u_{sz}}{\partial x^2}+\frac{\partial^2 u_{sz}}{\partial y^2}+\frac{\partial^2 u_{sz}}{\partial z^2}\right)+f_{sz} \quad (7)$$

The component forms of Eqs. (5) and (6) can be expressed as:

$$u_{sx}=u_{tx}\quad u_{sy}=u_{ty}\quad u_{sz}=u_{tz} \quad (8)$$

$$\sigma_{sx}=\sigma_{tx}\quad \sigma_{sy}=\sigma_{ty}\quad \sigma_{sz}=\sigma_{tz}$$
$$\tau_{sxy}=\tau_{txy}\quad \tau_{syz}=\tau_{tyz}\quad \tau_{szx}=\tau_{tzx} \quad (9)$$

Equation (7) is transformed by Laplace transformation for the time t and Fourier transformation for x, y and z, that is:

$$\tilde{u}(s,\omega_x,\omega_y,\omega_z)=\int_0^{+\infty}\int_{-\infty}^{+\infty}\int_{-\infty}^{+\infty}u(t,x,y,z)e^{-st}e^{-i\omega_x x}e^{-i\omega_y y}e^{-i\omega_z z}\mathrm{d}t\mathrm{d}x\mathrm{d}y\mathrm{d}z$$

The Eq. (7) can be transformed as:

$$\rho_s s^2\tilde{u}_x=-(\lambda+\mu)\omega_x(\omega_x\tilde{u}_x+\omega_y\tilde{u}_y+\omega_z\tilde{u}_z)-\mu(\omega_x^2+\omega_y^2+\omega_z^2)\tilde{u}_x+\tilde{f}_{sx}$$
$$\rho_s s^2\tilde{u}_y=-(\lambda+\mu)\omega_y(\omega_x\tilde{u}_x+\omega_y\tilde{u}_y+\omega_z\tilde{u}_z)-\mu(\omega_x^2+\omega_y^2+\omega_z^2)\tilde{u}_y+\tilde{f}_{sy}$$
$$\rho_s s^2\tilde{u}_z=-(\lambda+\mu)\omega_z(\omega_x\tilde{u}_x+\omega_y\tilde{u}_y+\omega_z\tilde{u}_z)-\mu(\omega_x^2+\omega_y^2+\omega_z^2)\tilde{u}_z+\tilde{f}_{sz} \quad (10)$$

Three vectors are defined as: $U=\left(\tilde{u}_x,\tilde{u}_y,\tilde{u}_z\right)^{\mathrm{T}}$, $\Omega=\left(\omega_x,\omega_y,\omega_z\right)^{\mathrm{T}}$, $F=\left(\tilde{f}_{sx},\tilde{f}_{sy},\tilde{f}_{sz}\right)^{\mathrm{T}}$. Equation (10) can be simplified as:

$$\rho s^2 U=-(\lambda+\mu)\Omega\Omega^{\mathrm{T}}U-\mu\Omega^{\mathrm{T}}\Omega U+F \quad (11)$$

Then U can be calculated as follows:

$$U=[\rho s^2 E_3+(\lambda+\mu)\Omega\Omega^{\mathrm{T}}+\mu\Omega^{\mathrm{T}}\Omega]^{-1}F \quad (12)$$

where E_3 is the 3 × 3 unit matrix.

Therefore, the displacement fields in time–space domain can be obtained by inverse Fourier transformation and inverse Laplace transformation with the contact conditions considered. Then the strain fields and stress fields can be obtained through Eqs. (1) and (2).

Numerical model

Model size

The numerical model in this paper is based on Subway Line 8 in Shanghai, 8–18 m in depth from the center of the tunnel to the ground surface. The external and inner diameters are 6.2 and 5.5 m, respectively. The characteristics of the tunnel were assumed to be the same, therefore a plane strain problem was considered and only one interception was chosen, as shown in Fig. 1. In order to compare the dynamic response of thawing soil and undisturbed soil, the numerical model was applied to simulate them, respectively. As the aim is to investigate the general differences of dynamic response between thawing soil and ordinary soil, a single kind of soil (thawing soil or undisturbed soil) was assumed around the tunnel to simplify the model. A, B and C in the model were taken as the reference points, as shown in Fig. 1.

Vibration load of the train

According to a lot of researches and tests of the Center of British Railway (Jenkins et al. 1974; Dawn and Stanworth 1979), the vertical force of the train vibration occurs mainly in the three ranges of frequency: the low frequency (0.5–5 Hz), the medium frequency (30–60 Hz) and the high frequency (200–400 Hz). The dominating frequency is the low frequency. According to the frequency ranges of

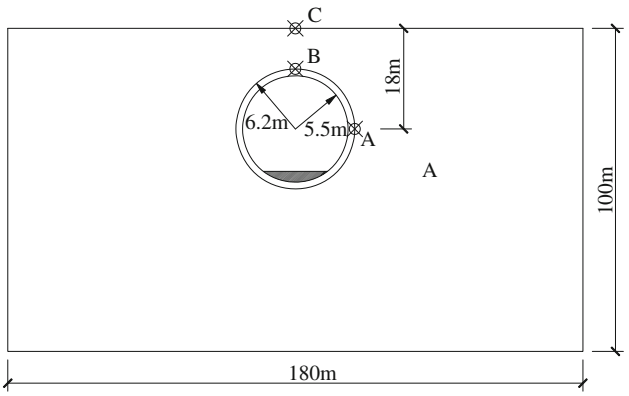

Fig. 1 Model size and the reference points

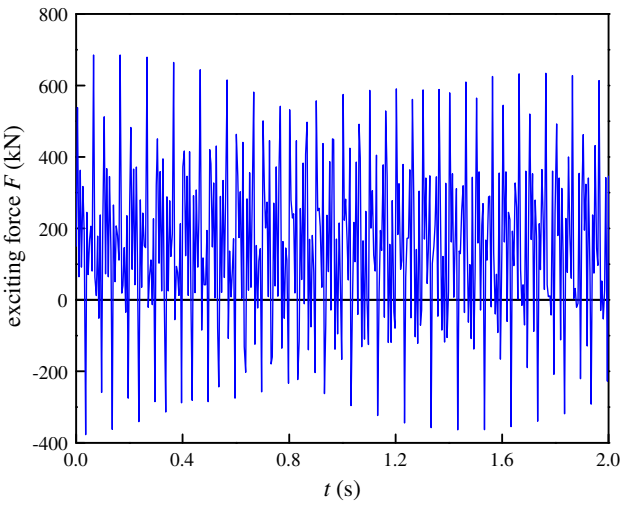

Fig. 2 The curve of the vibration force

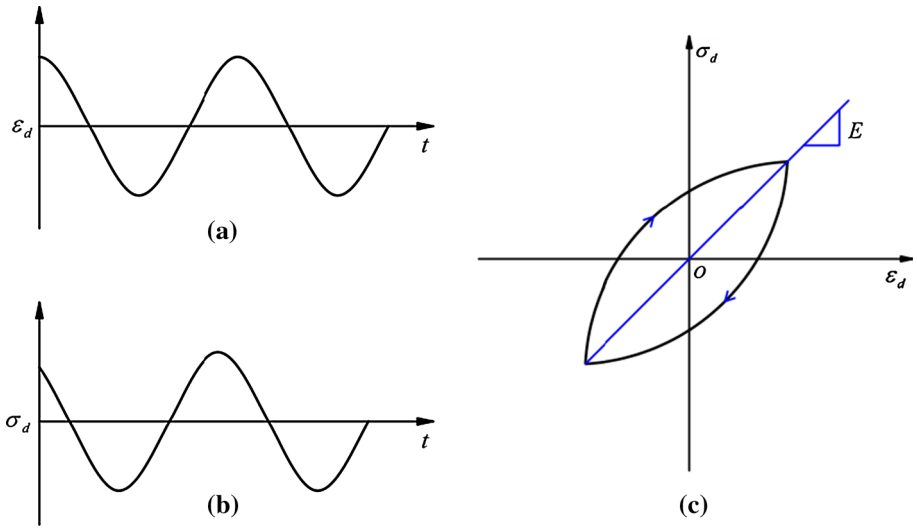

Fig. 3 The dynamic stress (**a**), the dynamic strain (**b**) and the hysteresis curve (**c**)

the load, the function of an exciting force can be adopted to represent the vibration load (Pan and Pande 1984):

$$F(t) = A_0 + A_1 \sin \omega_1 t + A_2 \sin \omega_2 t + A_3 \sin \omega_3 t \quad (13)$$

where A_1 is the static load of the wheel, A_2, A_3, A_4 are the peaks of the vibration loads which are corresponding to the circular frequencies ω_1, ω_2, ω_3, respectively.

According to the frequency ranges of the load, $A_0 = 1.5 \times 10^5$ N, $A_1 = 1.5 \times 10^5$ N, $A_2 = 1.6 \times 10^5$ N and $A_3 = 2.4 \times 10^5$ N. The corresponding circular frequencies are $\omega_1 = 126$ rad/s, $\omega_2 = 314$ rad/s and $\omega_3 = 503$ rad/s. The vibration time was 2 s. Based on Eq. (13), the curve of the vibration force is shown in Fig. 2.

Parameters of soil

The undisturbed soil was dark green silty clay taken from Layer No. 6 in Shanghai. The undisturbed soil was frozen to −20 °C, and then the thawing soil was obtained after the melting of the frozen soil in a pool with room temperature. The dynamic modulus of the two kinds of soil samples were both obtained by dynamic triaxial tests.

Because the soil is not an ideal elastomer, the dynamic stress (σ_d) and its corresponding dynamic strain (ε_d) are not synchronized, as shown in Fig. 3a, b. If the dynamic stress and the dynamic strain in a cycle are painted in the same coordinate plane, the hysteresis curve as shown in Fig. 3c can be gained. The average slope of the hysteresis curve is taken as the dynamic modulus E_d:

$$E_d = \sigma_{d_{\max}} / \varepsilon_{d_{\max}} \quad (14)$$

In the vibration of underground railway, the maximum strain is less than 10^{-4}, thus the dynamic modulus is assumed to be constant. The soil parameters obtained by the tests are summarized in Table 1.

Table 1 Parameters of soil

Soil\parameters	Undisturbed soil	Thawing soil	Segment
E (MPa)	270	250	35,000
μ	0.35	0.46	0.25
ρ (kg/m^3)	1,870	2,100	2,500

Damping parameter and boundary conditions

Since the presence of the damping and the radiation attenuation caused by the increment of propagation distance, waves will not propagate unlimited in soil medium. Damping is an important attribute of dielectric material, which cannot be ignored. In order to quantify the damping, Rayleigh damping was adopted.

Rayleigh damping can be expressed as:

$$[C] = \alpha[M] + \beta[K] \quad (15)$$

where $[M]$ is the mass matrix; $[K]$ is the stiffness matrix; α and β are the damping coefficients.

If the damping ratio ξ_i remains unchanged in a certain frequency range $\omega_i \sim \omega_j$, according to the orthogonal condition of vibration mode, the damping coefficients can be determined:

$$\alpha = \frac{2\omega_i\omega_j}{\omega_i + \omega_j}\xi \qquad \beta = \frac{2}{\omega_i + \omega_j}\xi \quad (16)$$

In order to determine the damping coefficients, two circular frequencies ω_i and ω_j are needed. The general idea is to carry out the analysis of the vibration mode and two modes are selected to calculate the damping coefficients. Because the vibration of the subway is mainly focused on

Table 2 Frequency of the thawing soil with different modes

Mode	1	2	3	4	5	6	7	8
Frequency (Hz)	0.9726	1.1800	1.8950	2.1046	2.5178	2.6242	2.7840	2.9178

Table 3 Frequency of the undisturbed soil with different modes

Mode	1	2	3	4	5	6	7	8
Frequency (Hz)	1.0152	1.3276	2.1077	2.3853	2.7722	2.8828	3.0459	3.1781

Table 4 Damping coefficients of the thawing soil and the undisturbed soil

Damping coefficient	α	β
Thawing soil	0.4583	0.0041
Undisturbed soil	0.4835	0.0038

the vertical vibration, two modes of the maximum participated mass of the vertical vibration were selected to determine the damping coefficients.

Above all, the analysis of the vibration mode was carried on. The front 200 modes of the thawing soil and the undisturbed soil were extracted, respectively. Frequencies of the thawing soil and the undisturbed soil with front 8 modes are summarized in Tables 2 and 3, respectively.

According to the results of the mode analysis, the modes of the maximum participated mass of the vertical vibration are No. 1 and No. 8. Assuming that the damping ratio remained constant, $\xi = 0.05$, according to Eq. (16), the damping coefficients of the thawing soil and the undisturbed soil can be calculated, as summarized in Table 4.

The viscous boundary conditions were conducted as the boundary conditions in this paper. Lysmer and Kuhlemeyer proposed the concept of viscous boundary in dashpots to absorb incident waves. The dashpots were added at the boundary of the tangential and normal directions. The viscous boundary tractions in the x and y directions are calculated by the following equations:

$$f_x = -\rho c_p \frac{\partial u}{\partial t} \qquad f_y = -\rho c_s \frac{\partial v}{\partial t} \tag{17}$$

where f_x and f_y are tractions applied to the boundary; ρ is the mass density; c_p and c_s are the velocities of P and S wave, respectively.

Analysis of results

Vibration acceleration of the thawing soil

Figure 4a, b, c and d illustrate the vibration acceleration of the thawing soil at 0.5, 1.0, 1.5 and 2.0 s, respectively.

From Fig. 4, the direction of wave propagation (the direction of energy propagation) is mainly downward along the bottom of the tunnel. The area of larger acceleration is mainly concentrated on the lower half of the tunnel, and it is a parabolic distribution. The acceleration at the contact position of the tunnel bottom between the soil and the segment experiences the maximum, which is about 50–60 m/s^2. However, with the increase of the distance from the bottom, the vibration acceleration decreases rapidly to be zero and the distance is about 10 m.

Amplitude-frequency curves of the displacements

The amplitude-frequency curves of the displacements can be obtained after Fast Fourier Transform (FFT) of the time-history curves of the point A, B and C, as shown in Fig. 5.

Comparing the displacement spectrograms of the thawing soil and the undisturbed soil at point A, B, and C, the main frequency range of the thawing soil is larger than that of the undisturbed soil. The frequency range of the thawing soil is 0–8 Hz, while that of the undisturbed soil is 0–4 Hz. There are two peak frequencies (2 and 6 Hz) for the thawing soil at point A, B and C, while there is only one (2 Hz) for the undisturbed soil. This shows that the wave in the soil decays quickly and it has been attenuated to be zero within a short distance.

Attenuation of the acceleration

Figure 6 illustrates the attenuations of the acceleration with the distance to the vibration source in the vertical direction at 2 s. From Fig. 6, the thawing soil and the undisturbed soil both decay exponentially and their attenuation formulas are obtained by exponential fitting, respectively, as shown in Table 5.

Figure 6 depicts that the position of the maximum acceleration is in the vicinity of the vibration source and the acceleration of each kind of soil decays to be zero within 10 m. According to the fitting formulas, the maximum acceleration of the thawing soil is approximately 63 m/s^2, while that of the undisturbed soil is just about 30 m/s^2, 48 % of the maximum acceleration of the thawing soil. Comparative analysis of the decay rates

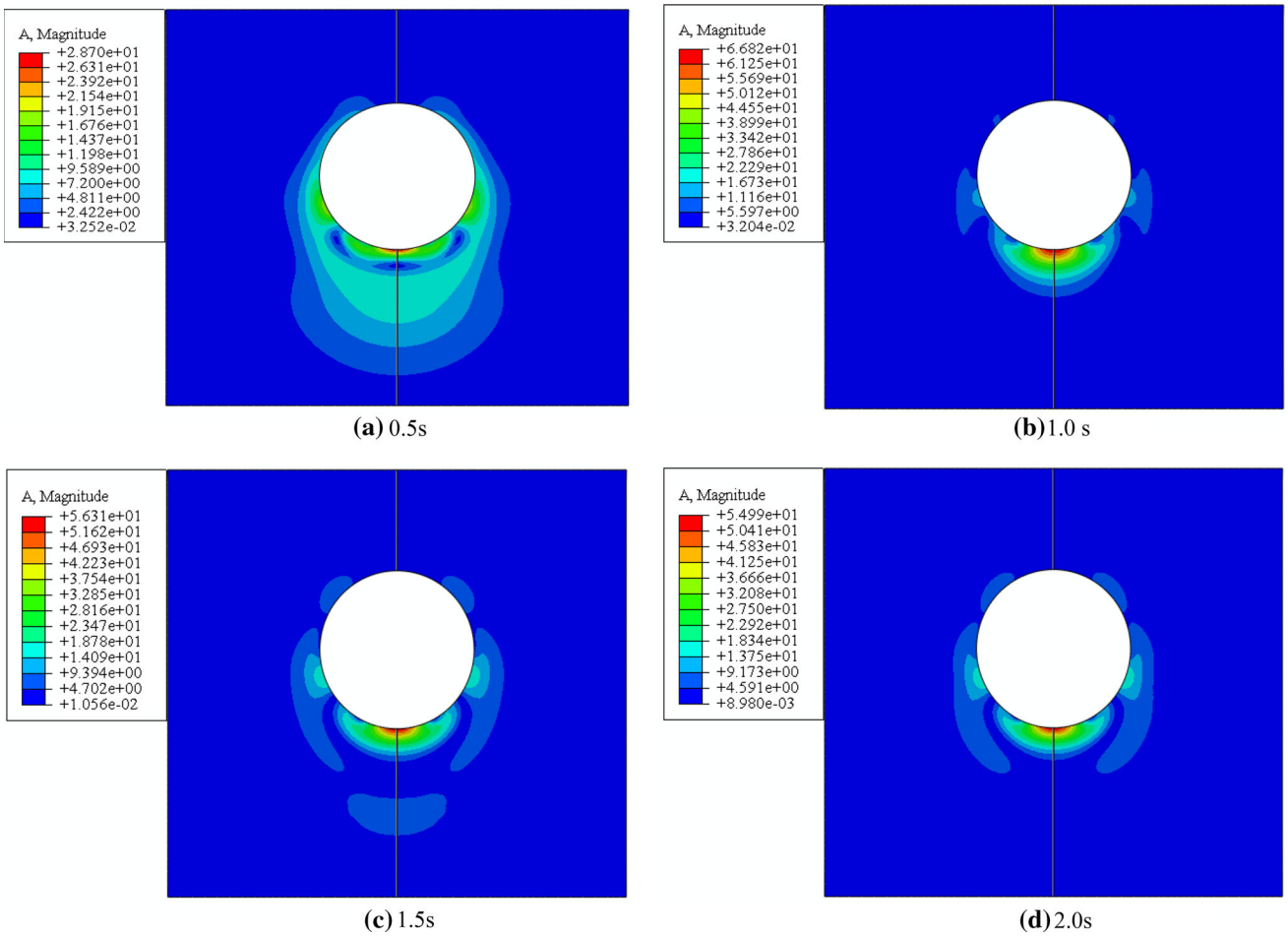

Fig. 4 Vibration acceleration of the thawing soil

shows that the attenuation coefficients of the thawing soil and the undisturbed soil are 0.7102 and 0.4295, respectively, the attenuation coefficient of the undisturbed soil being approximately 60 % of that of the thawing soil. Therefore, both the maximum vibration acceleration and the attenuation coefficient of the thawing soil are larger than those of the undisturbed soil. The main reason of the larger acceleration of the thawing soil is that the freezing and thawing decreases the elastic modulus and the internal soil particles are looser; the cause of the larger attenuation coefficient of the thawing soil is that the increase of the porosity enhances the absorption of vibration wave. The above analysis shows that the vibration acceleration of the thawing soil is approximately twice of that of the undisturbed soil. The soil near the segment directly affects the settlement and deformation of the tunnel. If the vibration acceleration is too large, the soil will be more prone to be damaged in the long-term cyclic loads, and the local stability of the tunnel will be affected.

The maximum ground acceleration and displacement

Figure 7 illustrates the variations of the maximum ground acceleration and the ground displacement with distance to the symmetry axis in 2 s. From Fig. 7a, the overall trend of the acceleration is decreasing, but there is a certain increase of the vibration acceleration of the thawing soil at 40–50 m, that is the vibration amplification appears. The reasons of the increase of the ground acceleration are that: (1) the Rayleigh wave emerges after the vibration waves propagate for a certain distance; (2) the waves with various frequencies attenuate inconsistent in the process of propagation.

The maximum ground accelerations that appear at the top of the tunnel, are approximately 1.48 and 0.92 m/s^2 for the thawing soil and the undisturbed soil, respectively. The maximum acceleration of the undisturbed soil is just about 62 % of that of the thawing soil. But at the same time, the acceleration of the thawing soil attenuates more rapidly and it attenuates to be near 0.3 m/s^2 when the distance reaches

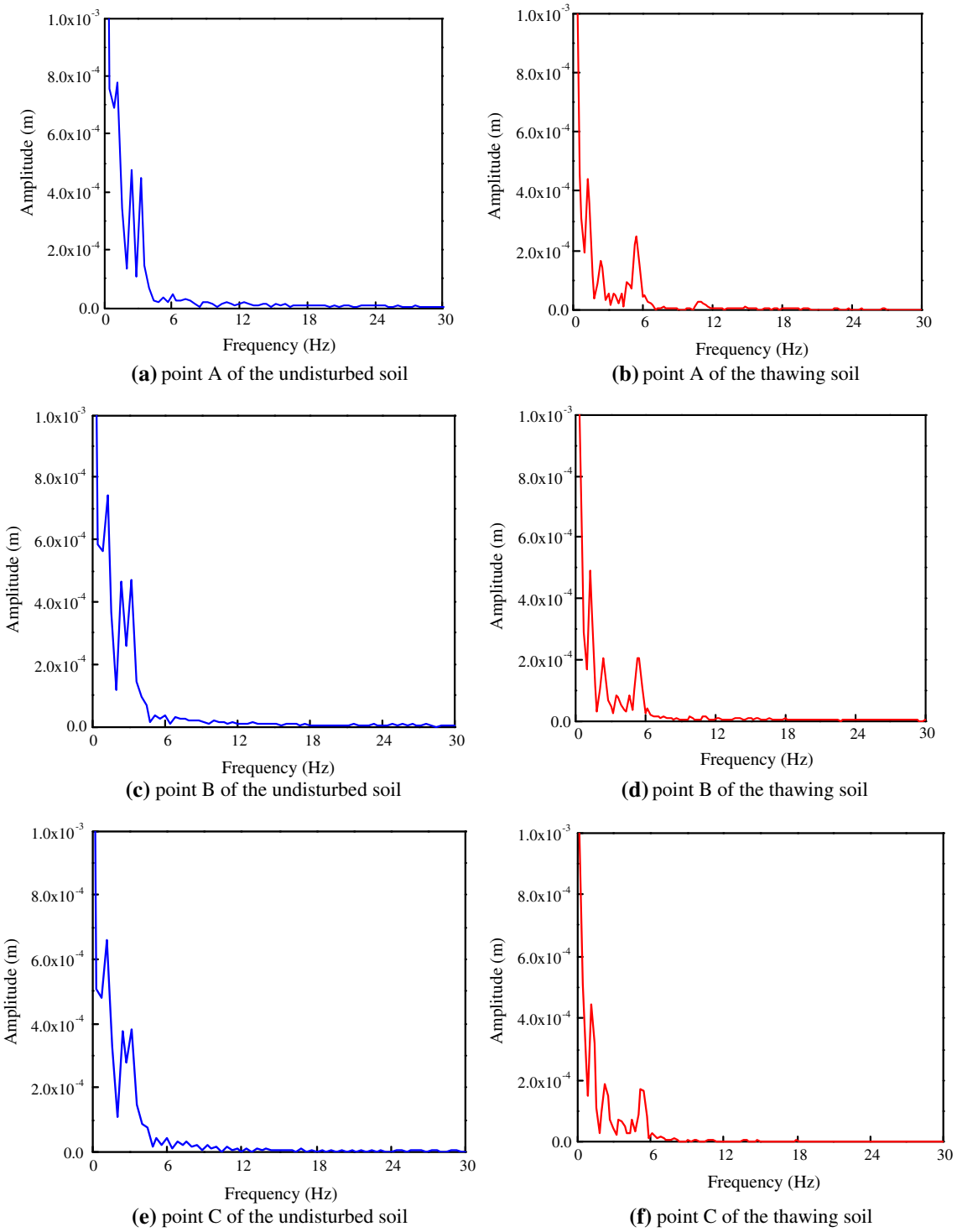

(a) point A of the undisturbed soil

(b) point A of the thawing soil

(c) point B of the undisturbed soil

(d) point B of the thawing soil

(e) point C of the undisturbed soil

(f) point C of the thawing soil

Fig. 5 Amplitude-frequency curves of the displacements at point A, B and C

20 m. The maximum ground acceleration of the undisturbed soil experiences a relatively smooth change and attenuates slowly, which maintains the magnitude between 0.3 and 0.6 m/s^2. The acceleration of the undisturbed soil is larger than that of the thawing soil when the distance to the symmetry axis is more than 10 m. Meanwhile, there is no obvious amplification region on the ground surface of the undisturbed soil.

From Fig. 7b, the maximum ground displacements of both the thawing soil and the undisturbed soil decrease to

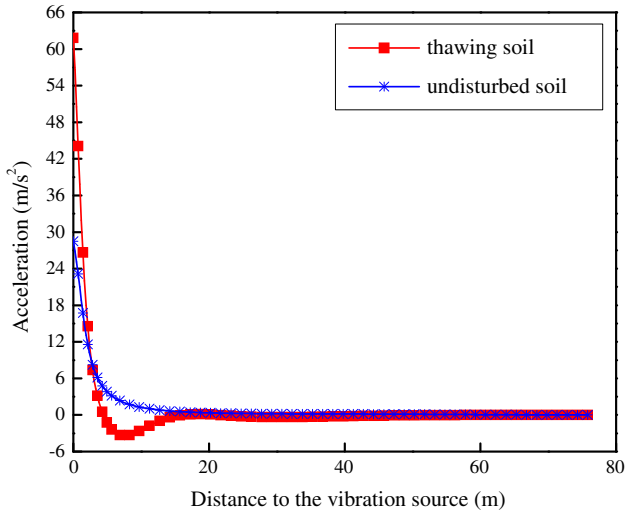

Fig. 6 Attenuation of acceleration with distance in the vertical direction

Table 5 Fitting results of the acceleration

Soil	Attenuation formulas
Thawing soil	$y = 68.2e^{-0.7102x} - 0.5315$
Undisturbed soil	$y = 29.57e^{-0.4295x} - 0.2209$

minimum and then increase. The displacements reach the minimum at 40–50 m away from the symmetry axis and the maximums appear at the top of the tunnel, which is about 3.0 mm. The minimum ground displacements of the thawing soil and the undisturbed soil are 1.4 and 1.1 mm, respectively. The changes of the maximum ground displacement of the thawing soil and the undisturbed soil are basically identical in the range 40–80 m, while the displacement of the thawing soil is larger than that of the undisturbed soil. The main reason why the curves in Fig. 7b increase after the minimum value is the same as that of Fig. 7a, namely Rayleigh wave emerges after the vibration waves propagate after the minimum value. As the energy of Rayleigh wave is mainly concentrated on the surface, the emergence of Rayleigh wave will evidently increase the ground displacement.

Time-history curves of the acceleration

The time-history curves of the acceleration of the thawing soil and the undisturbed soil at point A, B and C are shown in Fig. 8. To point A (Fig. 8a), there are not many differences between the thawing soil and the undisturbed soil, and the acceleration of each kind of soil fluctuates in the range of 2–12 m/s^2 to point B and C (Fig. 8b, c), the acceleration of the thawing soil is greater than that of the

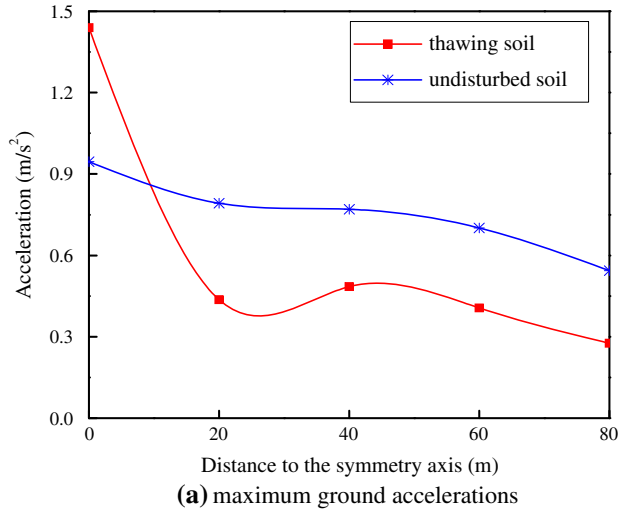

(a) maximum ground accelerations

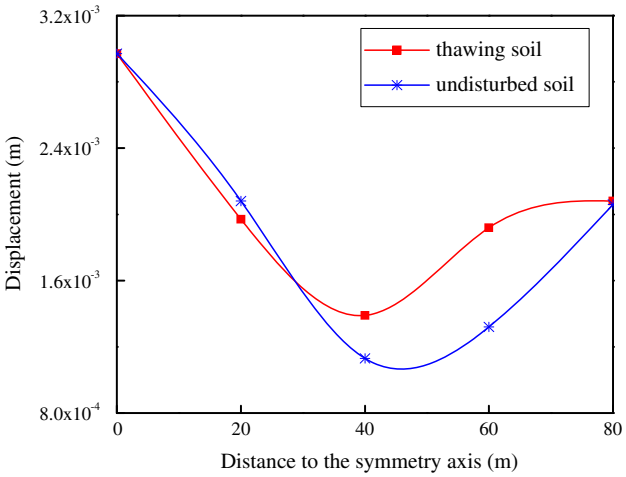

(b) maximum ground displacements

Fig. 7 Variations of the maximum ground accelerations and displacements with distance to the symmetry axis in 2 s

undisturbed soil. The main reasons are that the connecting forces between soil particles are weakened, and the elastic modulus and the strength of the soil reduce. Comparing the acceleration amplitudes of Fig. 8a, b and c, the acceleration amplitudes decrease gradually, which is the same as the conclusion of Fig. 7a.

Conclusions

(1) The direction of the wave propagation is mainly downward along the bottom of the tunnel. The area of larger acceleration is mainly concentrated on the lower half of the tunnel, and it is a parabolic distribution. The maximum acceleration is at the bottom contact position between soil and segment. But with the increase of the distance from the bottom, the vibration acceleration decreases rapidly to be zero.

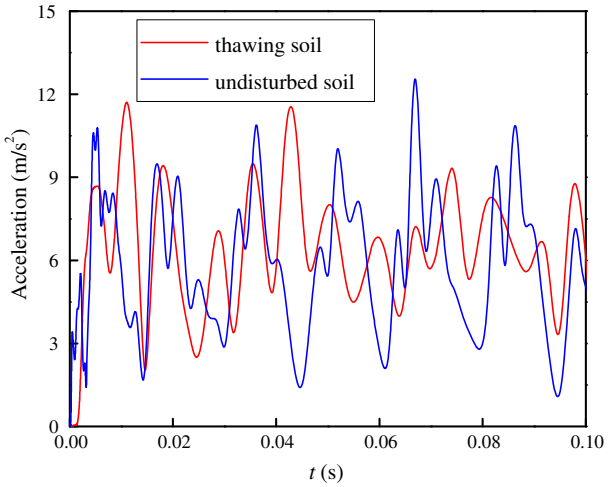

(a) point A

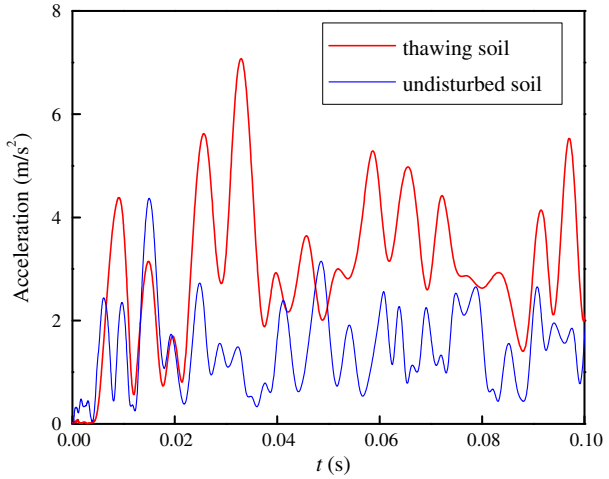

(b) point B

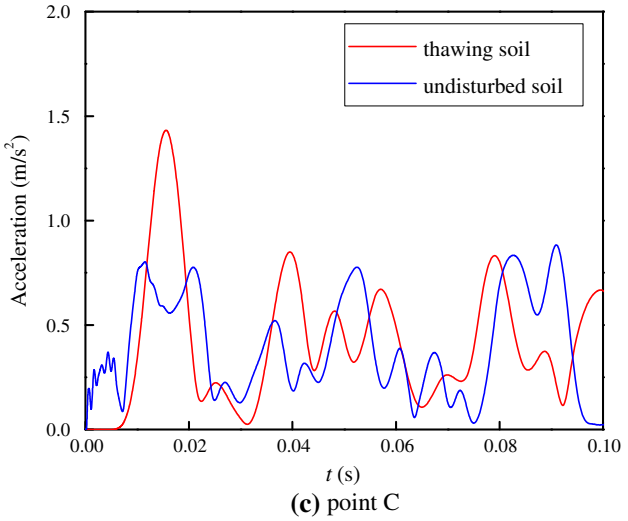

(c) point C

Fig. 8 Variations of the acceleration with time

(2) The main frequency range of the thawing soil is larger than that of the undisturbed soil at the corresponding points. The frequency range of the thawing soil is 0–8 Hz, and the frequency range of the undisturbed soil is 0–4 Hz. There are two peak frequencies (2 and 6 Hz) of the thawing soil, while there is only one (2 Hz) of the undisturbed soil.

(3) The position of the maximum acceleration is in the vicinity of the vibration source and the acceleration of each kind of soil decays to be zero within 10 m. The maximum acceleration of the thawing soil is approximately 63 m/s^2, while it is just about 30 m/s^2 (48 % of that of the thawing soil) of the undisturbed soil. The attenuation coefficients of the thawing soil and the undisturbed soil are 0.7102 and 0.4295, respectively. The attenuation coefficient of the undisturbed soil is approximately 60 % of that of the thawing soil. The maximum vibration acceleration and the attenuation coefficient of the thawing soil are both larger than those of the undisturbed soil.

(4) There is a certain increase of the vibration acceleration of the thawing soil at 40–50 m, while there is no obvious amplification region of the ground surface of the undisturbed soil. The maximum accelerations at the top of the tunnel are approximately 1.48, 0.92 m/s^2, respectively. The maximum acceleration of the undisturbed soil is just about 62 % of that of the thawing soil. But at the same time, the acceleration of the thawing soil attenuates more rapidly. It attenuates to be near 0.3 m/s^2 when the distance reaches 20 m. The maximum ground acceleration of the undisturbed soil experiences a relatively smooth change and attenuates slowly, which maintains the magnitude of 0.3–0.6 m/s^2. The acceleration of the undisturbed soil is larger than that of the thawing soil when the distance to the symmetry axis is more than 10 m.

(5) The maximum ground displacements of both the thawing soil and the undisturbed soil decrease to minimum and then increase. Each kind of soil reaches the minimum in the range of 40–50 m, and the maximum displacement appears at the top of the tunnel, which is about 3.0 mm. The minimum ground displacements of the thawing soil and the undisturbed soil are 1.4 and 1.1 mm, respectively. The changes of the maximum ground displacement of the thawing soil and the undisturbed soil are basically identical in the range of 40–80 m, while the displacement of the thawing soil is larger than that of the undisturbed soil.

(6) There are not many differences between the thawing soil and the undisturbed soil in the near field. But in the far field, as a result of the weaker connecting forces and smaller elastic modulus, the acceleration of the thawing soil is greater than that of the undisturbed soil.

Acknowledgments This work presented in this paper was supported by the National Natural Science Foundation of China (Grant No. 51208503), the Natural Science Foundation of Jiangsu Province, China (Grant No. BK2012133) and Qing Lan Project.

References

Alabi B (1992) A parametric study on some aspects of ground-borne vibrations due to rail traffic. J Sound Vib 153(1):77–87

Brams BB, Yao LYC (1964) Shear strength of a soil after freezing and thawing. J Soil Mech Found Div 90:1–25

Clouteau D, Arnst M, Al-Hussaini TM et al (2005) Freefield vibrations due to dynamic loading on a tunnel embedded in a stratified medium. J Sound Vib 283(1):173–199

Dawn TM, Stanworth CG (1979) Ground vibrations from passing trains. J Sound Vib 66(3):355–362

Dieterman HA, Metrikine V (1997) Steady-state displacements of a beam on an elastic half-space due to a uniformly moving constant load. European J Mech Series a Solids 16:295–306

Eason G (1965) The stresses produced in a semi-infinite solid by a moving surface force. Intern J Eng Sci 2(6):581–609

Ewing WM, Jardetzky WS, Press F (1958) Elastic waves in layered media. GFF 80(1):128–129

Finn WD, Yong RNY (1978) Seismic response of frozen ground. J Geotech Eng Div 104(10):1225–1241

Forrest JA, Hunt HEM (2006) A three-dimensional tunnel model for calculation of train-induced ground vibration. J Sound Vib 294:678–705

Graham J, Au VCS (1985) Effects of freeze-thaw and softening on a natural clay at low stresses. Can Geotech J 22(1):69–78

Guan F, Moore ID (1994) Three-dimensional dynamic response of twin cavities due to travelling loads. J Eng Mech 120(3):637–651

Hussein MFM, Hunt HEM (2007) A numerical model for calculating vibration from a railway tunnel embedded in a full-space. J Sound Vib 305:401–431

Israil ASM, Ahmad S (1989) Dynamic vertical compliance of strip foundations in layered soils. Earthq Eng Struc Dyn 18(7):933–950

Jenkins HH, Stephenson JE, Clayton GA et al (1974) The effect of track and vehicle parameters on wheel/rail vertical dynamic forces. Railway Eng J 3(1):2–16

Kaynia AM, Madshus C, Zackrisson P (2000) Ground vibration from high-speed trains: prediction and countermeasures. J Geotech Geoenviron Eng 126(6):531–537

Konrad JM (1989) Physical processes during freeze-thaw cycles in clayey silts. Cold Regions Sci Technol 16(3):291–303

Lieb M, Sudret B (1998) A fast algorithm for soil dynamics calculations by wavelet decomposition. Arch Applied Mech 68(3–4):147–157

Lu JF, Jeng DS, Lee TL (2007) Dynamic response of a piecewise circular tunnel embedded in a poroelastic medium. Soil Dyn Earthq Eng 27:875–891

Nejati HR, Ahmadi M, Hashemolhosseini H (2012) Numerical analysis of ground surface vibration induced by underground train movement. Tunn Undergr Space Technol 29:1–9

Pan CS, Pande GN (1984) Preliminary deterministic finite element study on a tunnel driven in loess subjected to train loading. J Civil Eng 17(4):18–28 (in Chinese with English abstract)

Rieckh G, Kreuzer W, Waubke H et al (2012) A 2.5 D-Fourier-BEM model for vibrations in a tunnel running through layered anisotropic soil. Eng Analysis with. Boundary Elements 36(6):960–967

Sheng X, Jones CJC, Thompson DJ (2002) Ground vibration generated by a harmonic load moving in a circular tunnel in a layered ground. In: Proceedings of the 10th International meeting on low frequency noise and vibration and its control, pp 83–96

Sheng X, Jones CJC, Thompson DJ (2006) Prediction of ground vibration from trains using the wavenumber finite and boundary element methods. J Sound Vib 293(3):575–586

Singh S, Donovan NC (1977) Seismic response of frozen-thawed soil systems. In: Proceedings of sixth world conference on earthquake engineering, Sarita Prakashan, Meerut, India, pp 2262–2226

Tang YQ, Yang Q, Yu H (2014) Changes of the pore distribution of silty clay under the subway train loads. Environ Earth Sci. doi:10.1007/s12665-014-3215-8

Ting JM, Martin RT, Ladd CC (1983) Mechanisms of Strength for Frozen Sand. J Geotech Eng 109(10):1286–1302

Viklander P, Eigenbrod D (2000) Stone movements and permeability changes in till caused by freezing and thawing. Cold Regions Sci Technol 31(2):151–162

Vinson TS, Li JC (1980) Dynamic properties of frozen sand under simulated earthquake loading conditions. In: Proceedings of the seventh world conference on earthquake engineering. Istanbul, pp 225–240

Vinson TS, Chaichanavong T, Czajkowski RL (1978) Behavior of frozen clays under cyclic axial loading. J Geotech Eng Div 104:779–780

Wolf JP (1985) Dynamic soil-structure interaction. Englewood Cliffs, Prentice-Hall int

Wolf JP (1988) Soil-structure interaction analysis in time domain. Prentice-Hall, Engle-wood Cliffs, NJ

Yan CL, Tang YQ, Liu YT (2013) Study on fractal dimensions of the silty soil around the tunnel under the subway loading in Shanghai. Environ Earth Sci 69:1529–1535

Yang P, Zhang T (2002) Research on the physical and mechanical properties of the artificial thawing soil. Glaciol 24(5):665–667 (in Chinese)

Yang YB, Hung HH, Chang DW (2003) Train-induced wave propagation in layered soils using finite/infinite element simulation. Soil Dyn Earthq Eng 23(4):263–278